

3D Switchable Diffractive Optical Elements Fabricated with Two-Photon Polymerization

John Sandford O'Neill, Patrick Salter, Zimo Zhao, Bohan Chen, Hassan Daginawalla, Martin J. Booth, Steve J. Elston, and Stephen M. Morris*

Direct laser writing is demonstrated by two-photon polymerization of multi-element diffractive optical components that can be switched on and off with an applied voltage. By exploiting the 3D capabilities of the laser microfabrication technique, multiple diffractive optical elements are written into a single liquid crystal (LC) layer. The switching behavior of the diffractive optical elements is controlled by simply changing the write-voltage of the anisotropic polymer structures during fabrication. Initially, 2D diffraction gratings are written at different depths within the LC layer. Each element is then activated by applying a voltage of sufficient amplitude that causes the second diffractive optical element to become inactive. This is then followed by a demonstration of multi-element computer generated holograms that are written at different depths within the LC layer. By altering the magnitude of the applied voltage, different images/patterns can be observed in the replay field using a simple electrode configuration. These compact and transmissive LC optical components could excel in applications where a degree of switchability is required but a highly pixelated fully programmable device is excessive.

Two-photon polymerization direct laser writing (2PP-DLW) is an additive manufacturing technique that allows free-form 3D writing of polymer microstructures in transparent photoresists.^[17–19] The ability to write in 3-dimensions is a result of the two-photon absorption process that occurs when a femtosecond laser is tightly focused in the photoresist material, which leads to the polymerization exclusively occurring in the focus of the laser in a small volume termed a voxel. By translating the sample with respect to the laser focus, 3D structures can be constructed voxel-by-voxel. With an appropriate selection of resist material and laser pulse energy, it is even possible to produce features with a resolution below the diffraction limit.^[20,21] A key area in the continuing development of 2PP-DLW is in the use of “smart” or functional resists, with growing interest in liquid crystalline (LC)

materials.^[22–25] We have previously demonstrated a polymerizable LC resist, where the properties of the final polymer material can be controlled during writing by the application of an electric field to change the molecular alignment.^[26–28] In this paper, we demonstrate the fabrication of electrically switchable multi-element DOEs that are encoded at different depths within the LC layer.

Due to the combination of their high birefringence and sensitivity to external fields, LCs have long found use as switchable optical materials in spatial light modulators (SLMs) and single-pixel switchable DOEs. LCOS (liquid crystal on silicon) SLMs, which were commercialized in the early 2000s, allow switching between arbitrary pixelated DOE designs with a switching speed of a few milliseconds.^[29] However, these pixelated devices are complex and require complementary metal-oxide-semiconductor (CMOS) backplane electronics to drive the individual pixels of the LC layer. For many tasks, it is more convenient to use single-pixel LC-DOEs which have a much simpler device architecture and a lower cost than SLMs. The earliest implementations of such optical elements employed a variety of conventional lithographic methods to pattern surface relief structures into standard negative photoresists before they were transformed into an active device by adding a layer of index-matched liquid crystalline material.^[30–36] For example, a previous study demonstrated a switchable DOE for use in textured surface inspection.^[30] In this case, a He-Cd laser was used to

1. Introduction

Diffractive optical elements (DOEs) are designed to manipulate the spatial distribution of light. They range from simple gratings that split a beam into a number of diffracted beams, to sophisticated computer-generated holograms (CGHs) that diffract light into a recognizable image.^[1] Applications of DOEs span across a vast number of industries and include holographic displays, augmented reality (AR)/virtual reality (VR), spectroscopy, aberration correction, beam steering, beam shaping, and 3D depth sensing.^[2–16]

J. Sandford O'Neill, P. Salter, Z. Zhao, B. Chen, H. Daginawalla, M. J. Booth, S. J. Elston, S. M. Morris
Department of Engineering Science
University of Oxford
Parks Road, Oxford OX1 3PJ, UK
E-mail: stephen.morris@eng.ox.ac.uk



The ORCID identification number(s) for the author(s) of this article can be found under <https://doi.org/10.1002/adom.202102446>.

© 2022 The Authors. Advanced Optical Materials published by Wiley-VCH GmbH. This is an open access article under the terms of the Creative Commons Attribution License, which permits use, distribution and reproduction in any medium, provided the original work is properly cited.

DOI: 10.1002/adom.202102446

write a DOE into a photoresist with a beam diameter of around 7 μm . A nematic LC was then placed on top of the DOE that was encoded into the photoresist. By adjusting the index of refraction of the LC, it enabled the device to switch between the normal system point spread function (PSF) and a Gaussian PSF. The fabrication of useful devices using approaches described to date is typically limited by complex multi-step fabrication processes or the resolution achievable. Furthermore, challenges exist in controlling the alignment of the LC on the fabricated polymer structures, with unwanted defects inhibiting the device performance.^[31]

Arguably the most successful switchable LC-DOE technology is holographic polymer dispersed LC (H-PDLC) which is formed by exposing a device containing a mixture of LC and photosensitive isotropic monomer to a UV interference pattern.^[37–39] However, a significant disadvantage of H-PDLC is that, compared to bulk LCs, large electric fields (15–20 V μm^{-1}) are required to switch off the diffraction, due to the confinement of the LC into micro- or nano-meter sized droplets.^[38,39] In response to this, a variation of H-PDLC called POLICRYPS (Polymer Liquid Crystal Polymer Slices) was developed by Caputo et al. that switches with external fields of just a few V μm^{-1} and provides diffraction efficiencies of up to 98%.^[40,41] Although the interference lithography fabrication process for H-PDLC/POLICRYPS is flexible and fast, it is limited to producing gratings that are on (i.e., produce a diffraction pattern) in the absence of an applied field. For some optical applications, including AR/VR, it is desirable to use gratings that do not consume power in the off-state and are therefore “hidden” and operate in “reverse-mode” (non-diffractive by default at 0 V).^[42] H-PDLC/POLICRYPS technologies are currently unable to provide a solution for such applications.

Previously reported reverse-mode LC-DOEs have been fabricated using interference of UV lasers to create a modulated intensity pattern that is encoded directly into a device containing a UV-sensitive polymerizable LC/reactive mesogen mixture.^[42,43] Applying a voltage to these devices after fabrication caused the LC in the unpolymerized channels to reorient, producing a refractive index mismatch between the polymer structures and the LC that results in diffraction. However, employing such holographic interference fabrication methods limits grating designs to simple periodic structures. Within these constraints, the most complex LC-DOEs created in this way have been 2D hexatic lattices of micropillars which produce hexatic diffraction patterns.^[43]

In this paper, 2PP-DLW is used for the first time to engineer electrically-switchable single-pixel 3D LC-DOEs with the ability to switch between two distinct diffraction modes. The strength of this approach lies in the ability of 2PP-DLW to perform fabrication in 3D, thereby enabling DOE designs with advanced functionality. Furthermore, it allows fabrication of polymer structures with an arbitrary spatial distribution, such that complex diffraction patterns can be produced from phase holograms fabricated into an LC device. Due to the freedom over the design of the phase patterns comprising these DOEs, and the additional degree-of-freedom offered by voltage-dependent 3D fabrication, both reverse-mode and conventional mode operation are achievable. As a result, these laser written elements have considerable potential to be used as next-generation switchable DOEs.

2. Results and Discussion

2.1. The Concept

In this study, we use a LC resist in a bespoke 2PP-DLW system in order to fabricate electrically-switchable LC-DOEs. The resist contains the nematic LC mixture, E7, which is doped with ≈ 30 wt% of the reactive mesogen RM257 and ≈ 1 wt% of the photoinitiator Irgacure 819. The mixture is held inside a glass device with planar indium tin oxide (ITO) electrodes that allow the application of a uniform electric field to the sample during and after fabrication. The inner surfaces of the cell are coated with a rubbed polyimide alignment layer that forces the LC into a homogeneous planar alignment in the absence of any other external stimuli. This mixture was capillary-filled into the LC cells, which were manufactured by Instec Inc, and the cell gap was determined by the diameters of the spacer beads.

The linear polarization of the fabrication laser was oriented perpendicular to the optical axis of the LC in order to avoid the focal splitting phenomenon that results from focusing a polarized beam through a birefringent material at high NA (see Figure S1, Supporting Information).^[44,45] When the resist undergoes 2PP, the reactive mesogen molecules crosslink via a free-radical polymerization reaction which stabilizes the molecular alignment of the LC at the moment of the exposure through the formation of a polymer network.^[23,27,28] The use of a DLW system allows for flexible patterning and rapid-prototyping, allowing us to fabricate complex DOE designs with relative ease. In this study, we use the 3D fabrication capabilities of 2PP-DLW to fabricate switchable bilayer LC-DOEs. These consist of two separate DOEs that are fabricated in the same region of an LC device but at different depths such that they are spatially separated in the direction normal to the substrates.

The principle behind the fabrication and operation of a bilayer LC-DOE comprised of two CGHs is illustrated in **Figure 1**. The fabrication procedure involves two simple steps. First, a voltage V_1 is applied to the device, and a binary-phase CGH (labeled “A” in Figure 1) is fabricated such that the polymer structures which represent the pixels of the CGH are tethered to the bottom substrate (Figure 1a). Following this, a voltage V_2 is applied to the device and the position of the laser focus is adjusted upward so that a second binary-phase CGH (labeled “B” in Figure 1) can be fabricated and tethered to the top substrate (Figure 1b). The application of a voltage causes the molecular alignment in the mixture to change, and the formation of a polymer network at a given voltage then stabilizes the alignment of the LC in that state.

After fabrication, the DOE is operated by illuminating the device with a collimated laser beam that is linearly polarized in a direction parallel to the optical axis of the LC mixture. The far-field diffraction pattern generated by the DOE can then be studied on a screen. When voltage V_1 is applied to the device, there is no contrast in the LC alignment between the polymerized pixels of CGH A (which were written at V_1) and the bulk of the cell (Figure 1c), so the incident light will see a uniform refractive index profile for CGH A and no diffraction will occur. In contrast, at this voltage V_1 , there is indeed a difference in the alignment between the polymerized pixels of CGH B and the bulk of the cell. This manifests as the incident light seeing

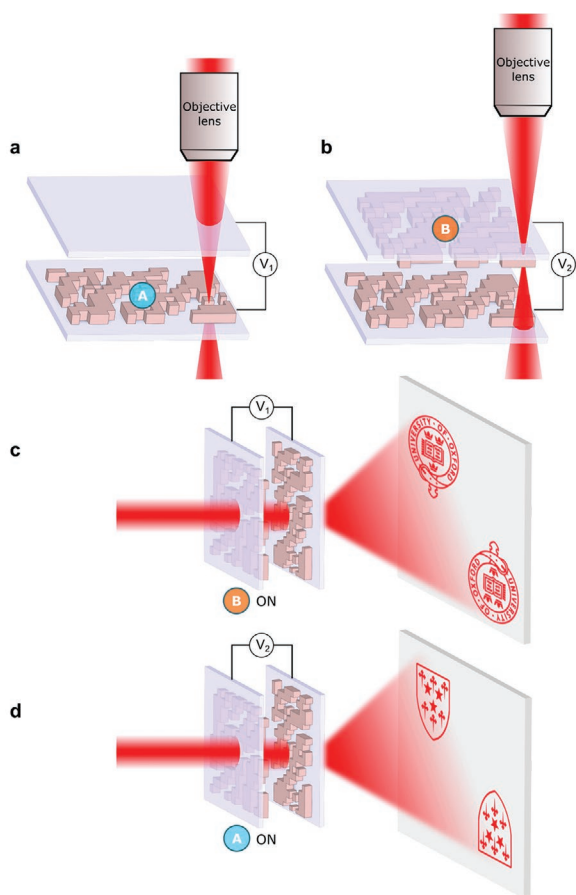


Figure 1. Schematic illustrations of the a,b) fabrication and c,d) operation of a bilayer switchable LC-DOE fabricated with 2PP-DLW. a) A computer-generated hologram (A) is fabricated inside a polymerizable liquid crystal device while the device is subjected to an applied voltage V_1 . The polymer structures that comprise the pixels of the CGH are tethered to the bottom substrate of the device and formed via two-photon polymerization. b) The focus of the fabrication laser is moved upward and a second CGH (B) is tethered to the top substrate and fabricated while a voltage V_2 is applied to the device. c) Post-fabrication, the device can be switched between two different states by applying the voltages used during fabrication. At a voltage V_1 , the CGH A is off and CGH B is on. d) At a voltage V_2 , CGH B is off and CGH A is on.

a spatially varying effective refractive index for CGH B which produces a diffraction pattern corresponding to CGH B in the far-field. Conversely, at voltage V_2 , the situation is reversed and CGH B is now off, CGH A is on, and the far-field diffraction pattern switches to that produced by CGH A alone. In this way, the LC-DOE can be switched between two different diffraction patterns post-fabrication by simply applying the write-voltages used during the fabrication of the device.

2.2. Bilayer Diffraction Elements

To begin with, we demonstrate the fabrication of two orthogonal gratings that are written at different depths within the LC device and activated using different voltages. Examples of 1D diffraction gratings (operating in both conventional and reverse mode) are presented in the Supporting Information (Figures S2–S6, Supporting Information). A schematic of a bilayer switchable

DOE is presented in Figure 2a. The polymer walls of grating A are fabricated such that they are tethered to the bottom substrate of the device and the polymer walls of grating B are tethered to the top substrate. This is a simple test-case of the proposed bilayer LC-DOE device architecture first introduced in Figure 1. This configuration is convenient because the diffraction patterns from each grating are easy to interpret and their orthogonality should be highly apparent. Figure 2b,c illustrates a schematic cross-section of the LC device during the fabrication process. The focus depth of the laser is changed during fabrication in order to tether the polymer structures to opposite substrates. In addition to the change in fabrication height, the voltage applied to the LC layer is also changed during the process so that the polymer walls comprising each grating are written at different voltages. Note that, for clarity in this schematic, grating A is shown being written at 0 V and grating B at an arbitrary voltage above the Fréedericksz threshold for the device, which is the voltage above which a reorientation of the LC director occurs.^[46,47] Voltage amplitudes below this threshold do not result in a reorientation of the LC director. In practice, however, it is not necessary that one of the fabrication voltages has to be 0 V.

The write-voltages used for fabricating each of the two gratings need to be carefully selected to ensure maximum diffraction efficiency for each grating. For maximum diffraction efficiency in a binary phase grating, the phase difference must be equal to π . Therefore, we need to find the relationship between phase and voltage for this device, such that the polymer structures of each grating can be written at two voltages with a phase difference equal to π . The phase as a function of voltage depends on the incident light wavelength (λ), the thickness of the LC device (d), and the birefringence of the mixture (Δn) and can be established experimentally in a straightforward manner by studying the transmissive behavior of the device when oriented between crossed polarizers. As is well known for a nematic LC between crossed polarizers, the transmission takes the form $T \propto \sin^2(\pi \Delta n d / \lambda)$, where the phase term relates directly to the birefringence Δn , thickness d , and wavelength λ . For 20 μm -thick devices illuminated at 635 nm, 3.7 V and 6.7 V were chosen as the write voltages for the two gratings (see Figure S7, Supporting Information).

It was necessary to use a cell thickness of 20 μm for bilayer LC-DOEs, in order to spatially separate the gratings in the direction normal to the cell substrates. Using a microscope objective with a numerical aperture (NA) of 0.45 the focal extent in the axial dimension is $\approx 10 \mu\text{m}$ while the lateral dimension of the voxel is $\approx 1 \mu\text{m}$. However, in order to ensure strong tethering of the polymer structures to the substrates, the focus depth of the fabrication laser was adjusted such that approximately half of the voxel was within the glass substrates. This results in localized polymer structures that are $\approx 1 \mu\text{m}$ in width and 5 μm in depth, as demonstrated in previous reports.^[26,27] Based upon these fabrication conditions, the minimum grating period that can be reliably fabricated using this approach is $\approx 2 \mu\text{m}$.

Figure 3 shows a sequence of polarized optical microscopy (POM) images of a bilayer LC-DOE under different applied voltage conditions with inset images of the corresponding diffraction patterns. The grating tethered to the bottom substrate, grating A, was written at 3.7 V with a grating period of 20 μm and has vertically-oriented polymer walls. Whereas grating B was tethered to the top substrate and was written at 6.7 V with

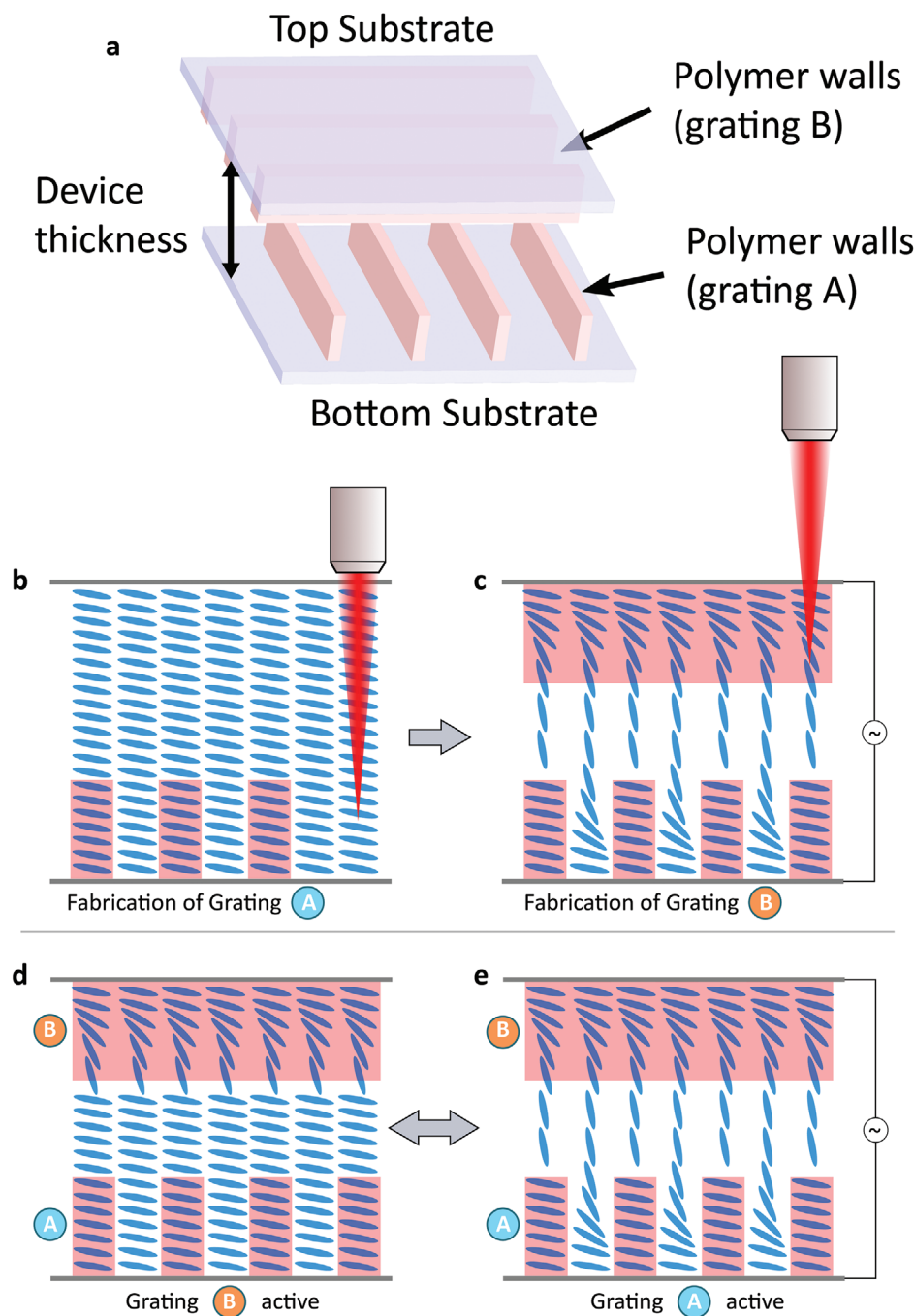


Figure 2. The fabrication and operation of a bilayer switchable DOE consisting of two orthogonal 1D diffraction gratings. a) Schematic showing the configuration of a bilayer switchable diffractive optical element. The polymer walls of grating A are tethered to the bottom substrate and the polymer walls of grating B are tethered to the top substrate. b) During the fabrication of grating A there is no voltage applied to the device and the polymer structures lock-in the LC alignment at 0 V. c) A voltage is then applied to the device, causing unpolymerized regions to switch. Grating B is then fabricated in the same region of the device but attached to the top substrate. Schematics showing the effect of voltage when switching between two gratings in the bilayer DOE. d) At 0 V, grating B (which was written with the voltage on) is active. e) Conversely, when the fabrication-voltage for grating B is applied to the device, grating A is active, as this grating was written at 0 V.

horizontally-oriented polymer walls of period 10 μm . At voltages near to the write-voltage for grating A (3.7 V), grating A is invisible in the POM images due to the homogeneity between the bulk director and the director of the polymer walls locked-in

at 3.7 V. Grating B is visible at these voltages because the polymer walls comprising grating B were locked-in at 6.7 V and therefore have a different director profile to the bulk at 3.7 V. The horizontally-oriented polymer walls of grating B are clearly

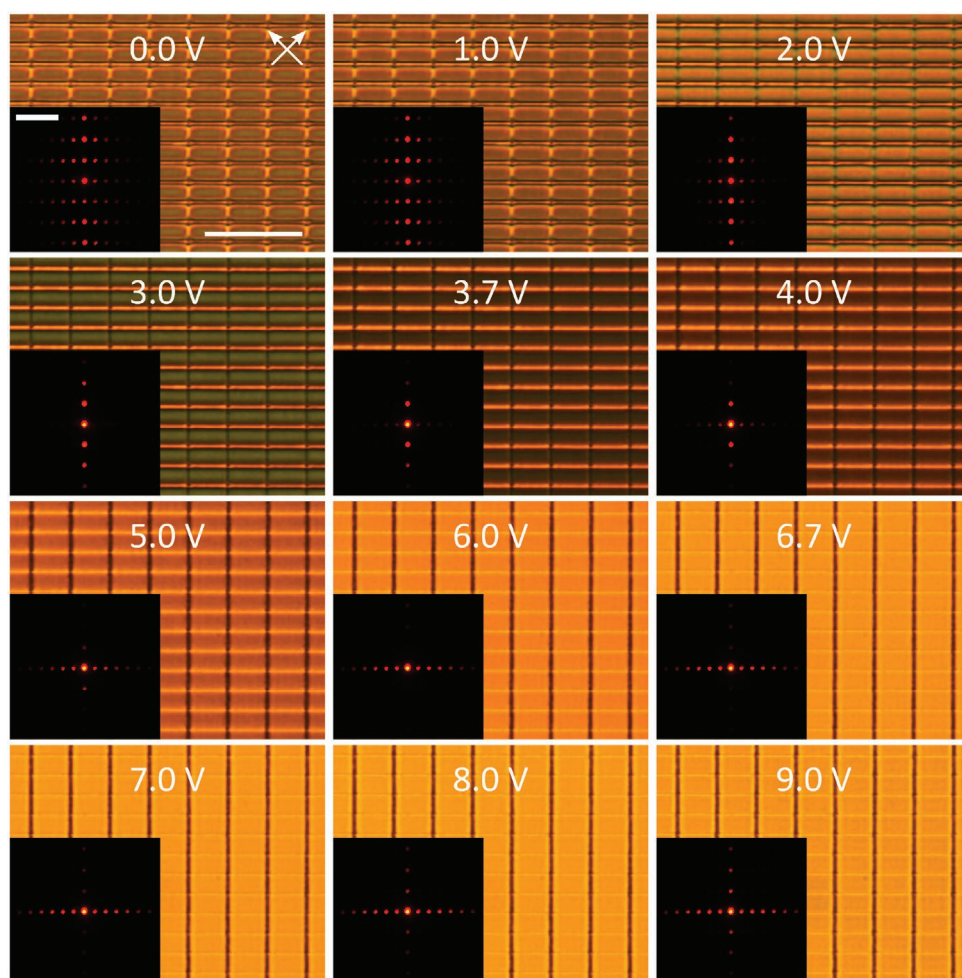


Figure 3. Polarised optical microscopy (POM) images of a bilayer DOE at a range of applied voltages, with inset images of the corresponding diffraction pattern at that voltage. Grating A had a pitch of 20 μm and was written at 3.7 V tethered to the bottom substrate, whereas grating B had a pitch of 10 μm and was written at 6.7 V tethered to the top substrate. Near to the writing voltages of 3.7 and 6.7 V, only one of the gratings is visible under POM and only one diffraction pattern can be seen. At other voltages, a mixture of the two gratings is observed. In these images the polymer walls of grating A are vertical whereas the polymer walls of grating B are horizontal. For the first image, the white arrows indicate the orientation of the crossed polarizers and the scale bar is 50 μm . The scale bar in the inset image (the replay field) is 2 cm.

visible in Figure 3 at voltages near to 3.7 V. At applied voltages near to the write voltage for grating B (6.7 V), grating B becomes invisible as the director in the bulk of the device is in the same director state as the polymer walls of grating B. Therefore, at these voltages, the vertically-oriented walls of grating A are visible due to the difference in the director alignment in the bulk of the device and the polymer walls of grating A, as can be seen in Figure 3 at voltages near to 6.7 V. Since the polymer structures lock-in the local director field at the point of exposure to the laser, and these anti-parallel-aligned devices exhibit no discontinuities in the director profile, therefore no defects or disclinations are observed around the polymer features.

On closer inspection, it appears that the diffraction pattern produced by grating B is in fact most visible at 3.0 V, rather than the writing voltage of 3.7 V. This effect is likely to be caused by the polymer walls written at 6.7 V exerting an elastic influence on the unpolymerized LC in the device. Locking-in this higher voltage creates an anchoring surface in the cell that influences

the adjacent bulk LC to match the alignment at 6.7 V which would effectively lower the index-matching voltage for grating A.

To highlight the freedom over the design of the gratings offered by 2PP-DLW, a more complex bilayer LC-DOE device is demonstrated in Figure S8, Supporting Information. In this device, one of the gratings is a triangular mesh of polymer walls and produces a hexatic diffraction pattern in the far-field and the other grating is a conventional 1D diffraction grating. The same cell thickness and write-voltages were used as in the LC-DOE in Figure 3. Grating A was comprised of periodic triangular elements with a pitch of 5 μm written at 3.7 V, while grating B was a 1D diffraction grating with a pitch of 5 μm written at 6.7 V. At applied voltages near to the write-voltage of the triangular mesh grating (3.7 V), only the 1D diffraction pattern produced by grating B is visible. As the voltage is increased toward the writing voltage of grating B (6.7 V), the pattern changes to the hexatic diffraction pattern produced by grating A.

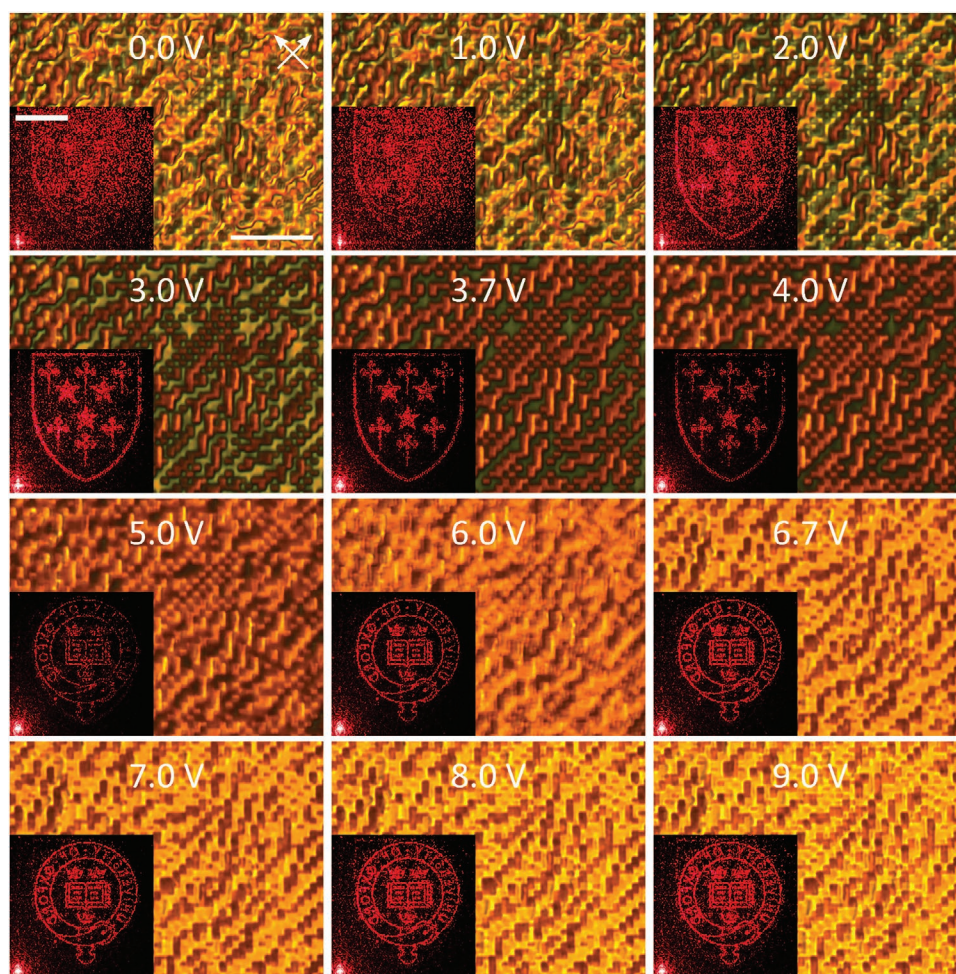


Figure 4. Polarized optical microscopy (POM) images of a bilayer computer generated hologram at a range of applied voltages, with inset images of the first order of the diffraction pattern at that voltage. The CGH that recreates the University of Oxford logo was written at 3.7 V tethered to the bottom substrate, whereas the CGH that recreates the Somerville College (Oxford) crest was written at 6.7 V tethered to the top substrate. Near to the writing voltages of 3.7 and 6.7 V, only one of the CGHs is visible under POM and only one of the diffraction patterns can be seen. The white arrows indicate the orientation of the crossed polarizers and the scale bar is 50 μm . The white scale bar in the first inset image (replay field) is 1 cm.

For devices with multiple DOE at different depths in the LC layer, achieving a configuration where incident light is completely unmodified by the device is extremely challenging, if not impossible. Even if none of the DOEs are active, the combination of the elements will lead to some form of diffraction pattern in the far-field, as can be seen in Figure 3 (for example at 0 V). This does, however, offer opportunities for further design potential, through considering how different layers interact with each other to diffract light when they are not actively addressed.

2.3. Multielement Computer Generated Holograms

A notable advantage to the use of 2PP-DLW for the fabrication of LC-DOEs is that we can exploit free-form patterning and create complex diffractive structures, such as holograms, with relative ease. Computer generated holograms (CGHs) are optical elements that produce a recognizable image in the far-field

diffraction pattern. The phase maps that define a hologram are highly aperiodic and 2PP-DLW is well-suited to the task of fabricating such a structure, due to the ability to arbitrarily control the exposure pattern of the writing laser.

POM images of a bilayer LC-DOE comprised of two binary CGHs are presented in Figure 4, with the inset images showing the far-field diffraction pattern. The designs of the CGHs were computed using the Gerchberg-Saxton algorithm (see Experimental Methods) and are shown in Figure S9, Supporting Information.^[48] CGH A was designed to recreate an image of the University of Oxford logo and was written at 3.7 V, whereas CGH B was designed to recreate an image of the Somerville College crest and was written at 6.7 V. This is the experimental realization of the bilayer CGH device first introduced conceptually in Figure 1. For completeness, results for a single layer CGH device are presented in Figure S10, Supporting Information.

The operation of the device is similar to the bilayer grating device shown in Figure 3, whereby applying the write-voltage

for a CGH renders it inactive. A real-time video of the diffraction pattern changing in response to the applied voltage can be seen in Movie S1, Supporting Information. For voltages close to 3.7 V, the write-voltage of the University of Oxford CGH, only the diffraction pattern from the Somerville College crest can be seen. Moreover, for voltages close to 6.7 V, the write-voltage of the Somerville College CGH, only the University of Oxford logo can be seen in the far-field. In this way, the diffraction pattern produced by the device can be switched between two distinct images by simply changing the magnitude of the voltage applied to the device. A plot of a “diffraction efficiency” is presented in Figure S11, Supporting Information. This was determined by calculating the complementary value of the ratio of the intensity of the zero-order spot recorded as a function of the applied voltage to that of the intensity of the laser spot when a non-laser written region was illuminated. For the mixture and devices used in this study, the rise and fall response times are found to be of the order of 100 and 700 ms, respectively, and are slightly lower for the laser-written polymerized regions compared with the non-polymerised regions of the device. Note that the relatively long response time is primarily due to the large device thickness (20 μm), and could be considerably reduced with a different LC cell geometry.

The bilayer DOEs presented in this study are the first demonstration of a new type of switchable LC diffraction grating. Although LCs have been widely used in switchable diffractive optics, previous technologies can typically only be switched between being on or off (i.e., producing a diffraction pattern, or not producing a diffraction pattern). In contrast, bilayer DOEs engineered with 2PP-DLW can be switched between two totally different diffractive states by exploiting the ability to laser write polymer structures at different voltages and on different layers within a device.

Another benefit of this approach to switchable DOEs is that the 2PP-enabled fabrication process supports multiple modes of operation. In many previously-reported LC diffraction gratings, including the industry-leading H-PDLC technology, fabricated devices are optically active by default (when no voltage is applied), such that a voltage is required to switch the device off. This is known as conventional mode. This limitation means that H-PDLC devices consume power in the off-state, which can be an undesirable characteristic for many applications where power consumption is an important design parameter. In contrast, with LC-DOEs made via 2PP-DLW, gratings can be engineered to operate in reverse-mode and be optically inactive with the voltage off, as demonstrated in Figure S2, Supporting Information, by simply writing the polymer structures at 0 V during fabrication. Gratings can also be designed to work in conventional mode (with the diffraction on by default at 0 V) by fabricating polymer walls at a voltage above the Fréedericksz threshold is applied to the device, as shown in Figure S3, Supporting Information. Therefore, in employing this fabrication technique for LC-DOEs, the grating designer is free to easily choose the mode of operation depending on the specific application and the desired switching properties of the DOE. In the future, mixture refinement may be required to prevent further cross-linking from taking place post fabrication if the samples are exposed to UV/blue light. For the samples used in this study, a relatively large concentration of reactive mesogen

has been employed. To mitigate this potential issue, it would be necessary to formulate mixtures consisting of a concentration of reactive mesogen/photoinitiator that better suits the volume of LC that should be polymerized by the laser writing process. This is something that we hope to explore in future work.

There are a number of contemporary applications of DOEs that could exploit the switchable LC-DOEs described in this study. LC-DOE gratings manufactured with 2PP-DLW could find use in 3D depth mapping technologies where gratings are used to create structured light illumination patterns. Versions of this technology, where DOEs are referred to as “dot projectors,” are found in Apple’s Face ID system and Microsoft’s Kinect, but are limited to producing a fixed dot grid to illuminate a scene. For the high-resolution depth sensing required to process the movements of individual fingers and subtle changes in facial expression, illumination grids of thousands of infrared dots are projected onto a scene of interest and processed by cameras and dedicated ASICs.^[49]

There are several methods disclosed in the prior art for optical 3D depth mapping using time-coded illumination, beam steering, and switchable DOEs.^[50–52] The bilayer LC-DOEs described in this study could find use in such applications as a switchable dot projector, able to project two different illumination patterns onto a scene. Alternatively, the 1D switchable diffraction gratings shown in Figures S2 and S3, Supporting Information would allow the light source to be switched between flood illumination and dot projection, which allows different sensors to collect multiple types of optical information with a single light source.^[53] There is an advantage in combining multiple optical functions in one switchable device, as many applications that use 3D depth mapping technology, including head-mounted displays, require extensive miniaturization and have stringent power consumption requirements. There is considerable potential for use of the bilayer CGH device architecture demonstrated in Figure 4 in advanced applications in holography. Stacked or “cascaded” CGHs have been used for applications including multiplexed information display, color images, and multiwavelength optical interconnects.^[54,55] Furthermore, stacked CGHs have been employed to improve image resolution and diffraction efficiency over conventional single-layer CGHs.^[56,57]

3. Conclusions

In this work, switchable multielement liquid crystal DOEs (LC-DOEs) have been demonstrated which have been fabricated using DLW. Results have been presented that show that sophisticated DOEs, in the form of CGHs, which can be made to appear with the application of a voltage across a very simple electrode structure that does not require complex drive circuitry. This presents a new device concept for compact and affordable DOEs that can be easily inserted into any optical system. By 3D structuring of the device with a polymer network at different depths in the liquid crystal (LC) layer, we can impart a different phase profile on the propagating light, which can then be tuned with different voltage amplitudes post-fabrication. The approach presented herein does not require complicated electrodes nor back-plane electronics and is therefore much simpler to produce compared with conventional SLM technologies.

The device is also fully transmissive so much easier to incorporate into an optical system.

In contrast to phase-only LCOS SLMs, which require complex active-matrix CMOS backplane electronics to drive the pixels of the LC layer, the multielement DOEs described here allow switching between different phase patterns in an incredibly simple single-pixel LC device with uniform ITO electrodes. They therefore have the potential to fill a critical gap that exists between fully-programmable SLM devices and fixed DOEs. This laser-written technology may first find use in applications where switching between different phase-profiles with a uniformly applied voltage provides more versatility than a static element that performs one function only yet avoids the full complexity (and cost) of high end SLM units. Here we present an approach that enables the fabrication of multi-functional optical elements that have a unique 3D profile.

4. Experimental Section

Preparation of Liquid Crystal Resist: The resist used for 2PP was a nematic LC mixture containing E7 (70.7 wt%), the reactive mesogen RM257 (Merck) (28.5 wt%), and photoinitiator Irgacure 819 (Merck) (0.8 wt%). This mixture was prepared via thermal mixing at 70 °C for 24 h before it was capillary-filled into anti-parallel rubbed LC cells manufactured by Instec Inc. The cells had planar ITO electrodes, allowing a uniform electric field to be applied to the LC mixture during and after fabrication. Cells with thicknesses of 5 and 20 μm were used in this study, with the cell gap maintained by spacer beads.

2PP-DLW: Femtosecond laser pulses with a pulse width of 100 fs from a Spectra-Physics Tsunami titanium-sapphire oscillator emitting at 780 nm with a repetition rate of 80 MHz were focussed with an Olympus 0.46 NA objective lens into the LC layer of the cell. The power of the fabrication laser was carefully adjusted such that it was just above the polymerization threshold, delivering the minimum necessary energy to the sample. This threshold power was found empirically to be 41 mW at a writing speed of 100 $\mu\text{m s}^{-1}$. The polarization of the laser was oriented to be perpendicular to the rubbing direction of the device with the aid of a half waveplate. Devices were mounted onto a stack of high-resolution translation stages (Aerotech ANT-95XY and ANT95V-3) with a positioning resolution of 1 nm. A halogen light source with a 550 nm long-pass filter was used to provide transmission illumination of the device so that the fabrication could be monitored in situ with a color CCD without affecting the photocuring process. Polymer walls were fabricated by moving the sample under continuous exposure to the pulsed laser beam at a speed of 100 $\mu\text{m s}^{-1}$. An arbitrary function generator (Tektronix AFG 3021) was used to apply square-wave AC voltages with a frequency of 1 kHz to the LC device during fabrication.

Optical Microscopy: Microscopy was conducted using an Olympus BX51 polarizing optical microscope with a QImaging Retiga R6 camera attached to the phototube. Olympus objective lenses were used with the cover slip correction collar set to the thickness of the glass slides comprising the LC device, to improve the quality of the images by reducing aberration. A long-pass filter with a cut-off wavelength of 550 nm was inserted between the halogen bulb and the sample to avoid causing any polymerization in the samples that still contained unreacted reactive mesogen molecules. Devices were oriented such that the rubbing direction was 45° to the transmission axes of the crossed polarizers by rotating the sample until the bright state was located. MATLAB scripts were written to automate the process of obtaining microscope images at a range of different voltages by controlling an arbitrary function generator (Tektronix AFG 3021) with SCPI commands. The microscope camera was controlled by a command library provided by the manufacturer.

Image Analysis of Microscope Images of Single-Layer Grating: The analysis was conducted by performing horizontal line-scans across a

greyscale version of the POM image of the grating under an applied field of 10 V (shown in Figure S2, Supporting Information). These line scans were averaged to reduce noise, and the result is plotted in Figure S5a, Supporting Information where each wall was represented by a peak. The scale was calibrated using a microscope calibration slide with an etched scale. The MATLAB function “findpeaks” was used to find the location of the peaks and these values are plotted against the peak number in Figure S5b, Supporting Information. An estimate of the polymer wall width can be obtained with an optional output from the “findpeaks” function, which calculates the full-width of the peak at half-prominence.

DOE Diffraction Characterization System: The DOEs in this study were characterized using the custom-built optical setup shown in Figure S6, Supporting Information. The light source was a 635 nm laser diode (Thorlabs PL202) which had a beam diameter of Ø3 mm and an optical power of 1 mW. To selectively illuminate a particular DOE within a device, the beam was shrunk by two lenses in a telescope configuration. For some DOEs written over a very small area, the beam had to be focussed with a 300 mm lens in order to produce a beam size small enough to fit entirely within the area of a structure. The output power of the laser diode was reduced to 100 μW with a variable ND filter to provide a suitable power for the CCD and photodiode. To allow targeting and positioning of the laser beam, the sample was mounted on a stack of precise manual translation stages (Thorlabs PT1) with a travel range of 25 mm in X and Y. To aid with locating and identifying DOEs in the device, a simple optical microscope was built, with illumination provided by a fiber-coupled 660 nm LED. A full-color CCD camera (Thorlabs DCC1240C) was used to provide a magnified image of the device so that it could be moved to the correct position.

The diffraction pattern could be recorded by either: (i) taking an image of the white screen using a full-color CCD (Thorlabs DCU224C) with a camera lens attached or (ii) recording the diffraction intensity directly with a photodiode (Thorlabs PDA36A-EC). MATLAB scripts were written to run voltage sweeps and automate the experimental process of obtaining diffraction data from DOEs. An arbitrary function generator (Tektronix AFG 3021) was controlled to provide the AC driving voltage to the DOE, while data was recorded by either the CCD focused on the screen or the photodiode. For the latter method, the voltage sweep had to be repeated for each diffracted order, realigning the photodiode between each measurement. The MATLAB script interfaced with the CCD camera via a .NET library, whereas the photodiode was connected to a digital oscilloscope (Tektronix TDS2024C) which was read via SCPI commands to return the voltage signal from the photodiode.

Electro-Optic Characterization of Liquid Crystal Resist: To select suitable voltages for the fabrication of the two gratings comprising a bilayer LC-DOE, the transmissive of an uncured device was studied as a function of voltage between crossed polarizers, with the optic axis of the device at 45° to the polarizers, using a laser diode of wavelength of 635 nm (Thorlabs PL202). The result of this is shown in Figure S7a, Supporting Information. The voltages of a peak and a trough in the transmission-voltage graph were then chosen. Peaks were where the device was effectively functioning as a half-waveplate, and the polarization was rotated by 90° from the polarizer axis to the analyzer axis. Troughs were where the device was functioning as a full-waveplate ($\lambda/2$ plate) and the polarization orientation was unchanged from the original orientation of the polarizer, resulting in extinction after the analyzer. The transmission of a birefringent layer between crossed polarizers, T , with its optic axis at 45° to the polarizer axes, can be related to phase, ϕ , through the equation, $T = \sin^2\left(\frac{\phi}{2}\right)$, where $\phi = \frac{2\pi\Delta n d}{\lambda}$. Note that this relation is, strictly speaking, the transmission normalised to the maximum transmission through the device. Using the above equation, the phase can be extracted from the transmission versus voltage (Figure S7b, Supporting Information).

CGHs: CGHs were produced using the Gerchberg-Saxton (GS) algorithm implemented in MATLAB. The target images for the bilayer CGH were a 512 × 512 pixel image of the Oxford University logo and a 300 × 300 pixel image of the Somerville College crest. These images were resized to 128 × 128 pixel images before being placed in the upper left corner of a black 256 × 256 pixel image. The reason for placing the

desired target in the upper corner of the input to the GS algorithm was to prevent overlap in the replay field with the zero-order spot and the conjugate image. The output of the GS algorithm was a 256×256 pixel binary hologram. The holograms were written with 2PP-DLW over an area of $1024 \times 1024 \mu\text{m}$, such that each pixel of the hologram was a size of $4 \times 4 \mu\text{m}$. The fabrication was performed in an LC cell of thickness $20 \mu\text{m}$. A MATLAB script converted the hologram designs into AeroBasic fabrication scripts which wrote the holograms line-by-line with a spacing of $1 \mu\text{m}$ between adjacent lines. The replay fields were captured with the aid of a Fourier lens to bring the far-field diffraction pattern to the plane of a CCD.

Supporting Information

Supporting Information is available from the Wiley Online Library or from the author.

Acknowledgements

J.S.O'N. gratefully acknowledges the Engineering and Physical Sciences Research Council (UK) and Merck for a Graduate Studentship (EP/N509711/1). P.S. gratefully acknowledges the Engineering and Physical Sciences Research Council (UK) for a Fellowship (EP/R004803/01). J.S.O'N. thanks Dr Jia-De Lin for useful discussions regarding this work. The authors also gratefully acknowledge The Royal Society and The John Fell Fund (Oxford) for financial support.

Conflict of Interest

The authors declare no conflict of interest.

Data Availability Statement

The data that support the findings of this study are available from the corresponding author upon reasonable request.

Keywords

computer generated holograms, diffractive optical elements, polymerizable liquid crystals, two-photon polymerization

Received: November 10, 2021

Revised: January 6, 2022

Published online: February 20, 2022

- [1] D. C. O'Shea, T. J. Suleski, A. D. Kathman, D. W. Prather, *Diffractive Optics: Design, Fabrication, and Test*, SPIE, Bellingham, WA **2003**.
- [2] A. Goncharsky, A. Goncharsky, S. Durlevich, *Opt. Express* **2016**, 24, 9140.
- [3] G. Li, D. Lee, Y. Jeong, J. Cho, B. Lee, *Opt. Lett.* **2016**, 41, 2486.
- [4] T. Levola, *J. Soc. Inf. Disp.* **2006**, 14, 467.
- [5] J. Xiong, K. Yin, K. Li, S.-T. Wu, *Adv. Photonics Res.* **2021**, 2, 2000049.
- [6] F. Kneubühl, *Appl. Opt.* **1969**, 8, 505.
- [7] E. G. Loewen, *J. Phys. E* **1970**, 3, 953.
- [8] K. D. Wulff, D. G. Cole, R. L. Clark, R. DiLeonardo, J. Leach, J. Cooper, G. Gibson, M. J. Padgett, *Opt. Express* **2006**, 14, 4169.
- [9] R. C. Dymale, *Opt. Eng.* **2005**, 44, 023201.

- [10] Z. He, F. Go, R. Chen, K. Yin, T. Zhan, S.-T. Wu, *Crystals* **2019**, 9, 292.
- [11] G. Račiukaitis, *J. Laser Micro/Nanoeng.* **2011**, 6, 37.
- [12] S. Katz, N. Kaplan, I. Grossinger, *Opt. Photonik* **2018**, 13, 83.
- [13] P. S. Salter, M. J. Booth, *Light: Sci. Appl.* **2019**, 8, 110.
- [14] J. Salvi, J. Pagès, J. Batlle, *Pattern Recognit.* **2004**, 37, 827.
- [15] J. Batlle, E. Mouaddib, J. Salvi, *Pattern Recognit.* **1998**, 31, 963.
- [16] A. S. Shpunt, Z. Zalevsky, US2008/010674A1, **2007**.
- [17] S. Kawata, H. B. Sun, T. Tanaka, K. Takada, *Nature* **2001**, 412, 697.
- [18] M. Malinauskas, M. Farsari, A. Piskarskas, S. Juodkazis, *Phys. Rep.* **2013**, 533, 1.
- [19] C. M. Soukoulis, M. Wegener, *Nat. Photonics* **2011**, 5, 523.
- [20] Z. Gan, Y. Cao, R. A. Evans, M. Gu, *Nat. Commun.* **2013**, 4, 2061.
- [21] J. Fischer, M. Wegener, *Laser Photonics Rev.* **2013**, 7, 22.
- [22] V. Hahn, F. Mayer, M. Thiel, M. Wegener, *Opt. Photonics News* **2019**, 30, 28.
- [23] H. Zeng, D. Martella, P. Wasylczyk, G. Cerretti, J.-C. G. Lavocat, C.-H. Ho, C. Parmeggiani, D. S. Wiersma, *Adv. Mater.* **2014**, 26, 2319.
- [24] S. Nocentini, F. Riboli, M. Burrelli, D. Martella, C. Parmeggiani, D. S. Wiersma, *ACS Photonics* **2018**, 5, 3222.
- [25] A. Münchinger, V. Hahn, D. Beutel, S. Woska, J. Monti, C. Rockstuhl, E. Blasco, M. Wegener, *Adv. Mater. Technol.* **2021**, 7, 2100944.
- [26] C. C. Tartan, P. S. Salter, T. D. Wilkinson, M. J. Booth, S. M. Morris, S. J. Elston, *RSC Adv.* **2017**, 7, 507.
- [27] C. C. Tartan, J. J. Sandford O'Neill, P. S. Salter, J. Aplinc, M. J. Booth, M. Ravnik, S. M. Morris, S. J. Elston, *Adv. Opt. Mater.* **2018**, 6, 1800515.
- [28] J. J. Sandford O'Neill, P. S. Salter, M. J. Booth, S. J. Elston, S. M. Morris, *Nat. Commun.* **2020**, 11, 2203.
- [29] Z. Zhang, Z. You, D. Chu, *Light: Sci. Appl.* **2014**, 3, e213.
- [30] M. Stalder, P. Ehbets, *Opt. Lett.* **1994**, 19, 1.
- [31] G. Lester, A. Strudwick, S. Coulston, *Opto-Electron. Rev.* **2004**, 12, 313.
- [32] C. Slinger, P. Brett, V. Hui, G. Monnington, D. Pain, I. Sage, *Opt. Lett.* **1997**, 22, 1113.
- [33] X. Wang, D. Wilson, R. Muller, P. Maker, D. Psaltis, *Appl. Opt.* **2000**, 39, 6545.
- [34] A. Xie, T. Ito, D. A. Higgins, *Adv. Funct. Mater.* **2007**, 17, 1515.
- [35] M. Fleisch, S. Gao, D. Bošnjaković, X. Zhang, R. A. Rupp, I. Drevenšek-Olenik, *Liq. Cryst.* **2019**, 46, 2075.
- [36] C. H. Lee, H. Yoshida, Y. Miura, A. Fujii, M. Ozaki, *Appl. Phys. Lett.* **2008**, 93, 173509.
- [37] K. Tanaka, K. Kato, S. Tsuru, S. Sakai, *J. Soc. Inf. Disp.* **1994**, 2, 37.
- [38] G. P. Crawford, *Opt. Photonics News* **2003**, 14, 54.
- [39] Y. J. Liu, X. W. Sun, *Adv. Optoelectron.* **2008**, 2008, 684349.
- [40] R. Caputo, L. De Sio, A. Veltri, C. Umeton, A. V. Sukhov, *Opt. Lett.* **2004**, 29, 1261.
- [41] R. Caputo, A. DeLuca, L. De Sio, L. Pezzi, G. Strangi, C. Umeton, A. Veltri, R. Asquini, A. d'Alessandro, D. Donisi, R. Beccherelli, A. V. Sukhov, N. V. Tabiryan, *J. Opt. A: Pure Appl. Opt.* **2009**, 11, 024017.
- [42] L. De Sio, P. F. Lloyd, N. V. Tabiryan, T. J. Bunning, *ACS Appl. Mater. Interfaces* **2018**, 10, 13107.
- [43] P. Kossyrev, M. E. Sousa, G. Crawford, *Adv. Funct. Mater.* **2004**, 14, 1227.
- [44] S. Stallinga, *J. Opt. Soc. Am. A* **2001**, 18, 2846.
- [45] G. Zhou, A. Jesacher, M. Booth, T. Wilson, A. Ródenas, D. Jaque, M. Gu, *Opt. Express* **2009**, 17, 17970.
- [46] V. Fréedericksz, A. Repiewa, *Z. Phys.* **1927**, 42, 532.
- [47] V. Fréedericksz, Z. Zolina, *Trans. Faraday Soc.* **1933**, 29, 919.
- [48] R. W. Gerchberg, W. O. Saxton, *Optik* **1972**, 35, 237.
- [49] B. Freedman, A. Shpunt, M. Machline, Y. Arieli, US8150142B2, **2007**.
- [50] A. Shpunt, US9066087B2, **2011**.
- [51] C. L. Niclass, A. Shpunt, G. A. Agranov, M. C. Waldon, M. A. Rezk, T. Oggier, US10324171B2, **2015**.

- [52] S. Borgsmüller, S. Noehte, C. Dietrich, T. Kresse, R. Männer, *Appl. Opt.* **2003**, 42, 5274.
- [53] T. Kämpfe, E.-B. Kley, A. Tünnermann, in *Adaptive Optics: Analysis and Methods/Computational Optical Sensing and Imaging/Information Photonics/Signal Recovery and Synthesis Topical Meetings*, OSA Technical Digest (CD) **2007**, <https://doi.org/10.1364/DH.2007.DTuD8>.
- [54] T. Kämpfe, E.-B. Kley, A. Tünnermann, P. Dannberg, *Appl. Opt.* **2007**, 46, 5482.
- [55] X. Deng, R. T. Chen, *Opt. Lett.* **2000**, 25, 1046.
- [56] E. Buckley, A. Cable, N. Lawrence, T. Wilkinson, *Appl. Opt.* **2006**, 45, 7334.
- [57] D. Chambers, G. Nordin, S. Kim, *Opt. Express* **2003**, 11, 27.